Available online at www.sciencedirect.com

SCIENCE DIRECT®

Chemical Physics Letters 377 (2003) 279–285

CHEMICAL PHYSICS LETTERS

www.elsevier.com/locate/cplett

Active phase for inclined CO_2 desorption on Rh(1 1 0) in steady-state CO oxidation

Izabela Rzeźnicka [a], Tatsuo Matsushima [b],*

[a] *Graduate School of Environmental Earth Science, Hokkaido University, Sapporo 060-0810, Japan*
[b] *Laboratory of Surface Reaction Dynamics, Catalysis Research Center, Hokkaido University, Sapporo 060-0811, Japan*

Received 3 March 2003; in final form 16 June 2003

Abstract

The angular and velocity distributions of desorbing CO_2 and LEED spot intensities were examined in steady-state CO oxidation on Rh(1 1 0) and Pd(1 1 0). On Rh(1 1 0), in the limited CO pressure range, the angular distribution splits into bi-directional lobes collimating at ±24° off normal along the [0 0 1] direction and the meta-stable (1 × 2) structure stabilized by oxygen is maximized. On the other hand, neither inclined CO_2 desorption nor meta-stable (1 × 2) was found on Pd(1 1 0).

1. Introduction

A (1 1 0) plane of noble metals is frequently reconstructed into missing-row forms with or without adsorbates [1]. The resultant surface commonly consists of three- or four-atom-wide microfacets with a (1 1 1) structure declining alternatively about +30° or −30° in the [0 0 1] direction [2]. The repulsive force exerting from its formation site to the product CO_2 in CO oxidation on noble metals is strong enough to hold the site orientation in the angular distributions [3]. In fact, reactive CO_2 desorption in thermal desorption experiments collimates fairly along the local normal of declining microfacets on reconstructed Pt(1 1 0) and Ir(1 1 0), indicating the CO_2 formation on inclined (1 1 1) facets [4,5]. On the other hand, no inclined CO_2 desorption was found on Pd(1 1 0) [6] and Rh(1 1 0) [7]. In this Letter, the presence of inclined CO_2 reactive desorption on Rh(1 1 0) during steady-state CO oxidation is reported for the first time.

In steady-state CO oxidation on Pt(1 1 0), reactive CO_2 desorption collimates fairly along the local normal of those declining facets even when the surface is mostly converted from the (1 × 2) into the (1 × 1) form [8]. Furthermore, the CO_2 desorption shifts to the surface normal at low CO pressures where the (1 × 2) surface is highly covered by oxygen [9]. The observation of inclined CO_2 desorption requires low-oxygen

---

* Corresponding author. Fax: +81-11-706-4748.
E-mail address: tatmatsu@cat.hokudai.ac.jp (T. Matsushima).

0009-2614/$ - see front matter © 2003 Elsevier B.V. All rights reserved.
doi:10.1016/S0009-2614(03)01169-2

coverage conditions. In the steady-state CO oxidation on Pd(1 1 0), however, no splitting CO_2 desorption is found in the temperature range from 420 to 500 K below the kinetic transition (KT), although the c(2 × 4)-O lattice due to the missing-row structure is observed [10–12]. The lack of inclined CO_2 desorption on this surface may be due to the instability of the (1 × 2) reconstruction without oxygen above 355 K [13]. On the other hand, the (1 × 2) reconstruction on Rh(1 1 0) has been reported to be stable up to 480 K [14]. STM work indicates that oxygen on Pd(1 1 0) and Rh(1 1 0) forms O–Rh–O–Rh zigzag chains extending along the $[1\bar{1}0]$ direction [12,15]. Such oxygen is not reactive enough to induce inclined CO_2 desorption. Thus, the inclined desorption on Rh(1 1 0) (1 × 2) might be observed at low-oxygen coverage conditions with high CO_2 formation up to 480 K. These conditions can be obtained just below the KT in steady-state CO oxidation [16]. Angular and velocity distribution measurements under such limited conditions can be performed by means of steady-state angle-resolved measurements [17,18].

2. Experimental

The apparatus consists of a reaction chamber, a chopper house, and an analyzer [17]. All the chambers were evacuated by individual pumping systems. The reaction chamber has XPS and LEED optics, an Ar^+ gun, and a quadrupole mass spectrometer (QMS) for the angle-integrated (AI) signal. In the chopper house, a cross-correlation chopper was rotated at 98.04 Hz, yielding a time resolution of 20 μs. Another QMS in the analyzer detected the angle-resolved (AR) signal. A Rh(1 1 0) or Pd(1 1 0) single crystal was rotated to change the desorption angle (θ; polar angle) in a plane including the [0 0 1] direction [3–5]. The partial pressures of ^{13}CO (P_{CO}) and O_2 (P_{O_2}) were kept constant by dosing gases continuously. Hereafter, the isotope ^{13}C is simply designated as C in the text. The LEED patterns were taken over a long integration because of the reduced beam current to the level of non-visible spots.

3. Results and discussion

3.1. Rh(1 1 0)

3.1.1. Kinetics

The steady-state CO_2 formation rate on Rh(1 1 0) became observable above the surface temperature (T_S) of 400 K and was maximized at around 480 K. Its CO pressure (P_{CO}) dependence changed sharply below the KT. The reaction showed a first order in CO at low P_{CO}, and with increasing P_{CO} in the middle of the active region (below the KT), the CO_2 formation per P_{CO} increased about twice and showed a rapid decrease above the KT (Fig. 1). Such kinetic behavior was observed in the pressure range from 1×10^{-7} to 1×10^{-5} Torr.

3.1.2. Angular distributions

The above enhancement of CO_2 desorption was remarkable at $\theta = 24°$. The AR signal at $\theta = 24°$ runs below that at $\theta = 0°$ at lower P_{CO} values (Fig. 2a), and, around the middle of the active region, it overcomes the other. The former is

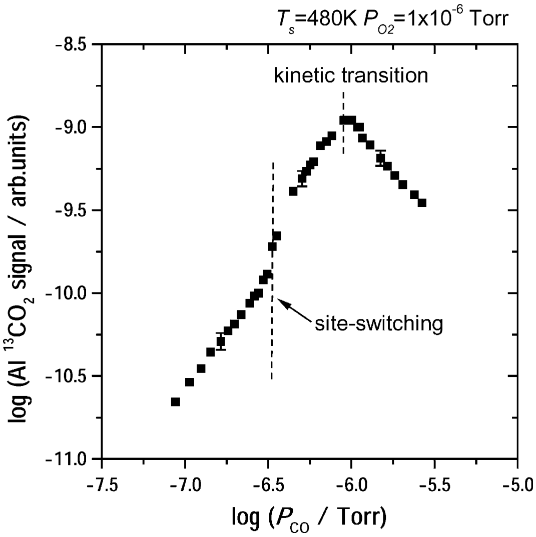

Fig. 1. Variation of the (AI) steady-state CO_2 desorption observed with CO pressures at $T_S = 480$ K and $P_{O_2} = 1.0 \times 10^{-6}$ Torr. The rate was determined by QMS in the reaction chamber as the difference in the CO_2 signal between the desired surface temperature and room temperature. Typical experimental errors are indicated by bars.

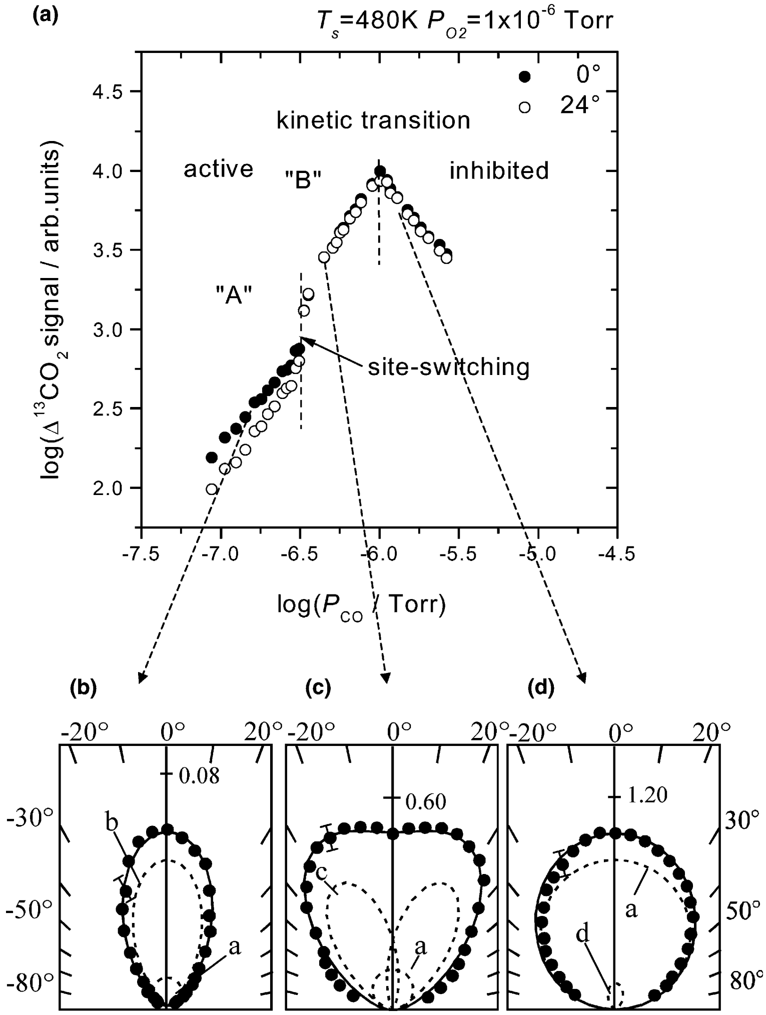

Fig. 2. (a) Variation of the (AR) steady-state CO_2 desorption observed at $\theta = 0°$ (•) and 24° (○) with CO pressures at $T_S = 480$ K and $P_{O_2} = 1.0 \times 10^{-6}$ Torr. The CO_2 formation rate was determined by QMS in the analyzer as the difference between the signal at desired angle and that when the crystal was away from the line-of-sight position. (b–d) Angular distributions of CO_2 in the plane along the [0 0 1] direction and typical deconvolutions are shown in polar coordinates. The ordinate was normalized to the signal in the normal direction at the inset (d). P_{CO} is: (b) 1.7×10^{-7} Torr, (c) 4.0×10^{-7} Torr, and (d) 1.50×10^{-6} Torr. The components drawn by broken curves show: (a) $\cos\theta$, (b) $\cos^6\theta$, (c) $\cos^8(\theta \pm 24°)$, and (d) $\cos^4\theta$. The solid curve is the summation of the components. Typical experimental errors are indicated by bars.

named 'active A,' and the latter, 'active B.' The boundary at which the CO_2 signal at $\theta = 24°$ becomes equal to that at $\theta = 0°$ is called 'site switching (SS)' [8,9]. At P_{CO} below this point, CO_2 desorption sharply collimated along the surface normal in a $\cos^4\theta$ form by considering a single component. The observed distribution above the SS in 'active B' became broader than a cosine form. It actually split into a bi-directional form (Figs. 2b, c). In the inhibited region, the signal closely followed a cosine distribution, as $\cos^{1.4}\theta$ (Fig. 2d).

3.1.3. *Velocity distribution*

In the three regions with different angular distributions, we examined the velocity distributions

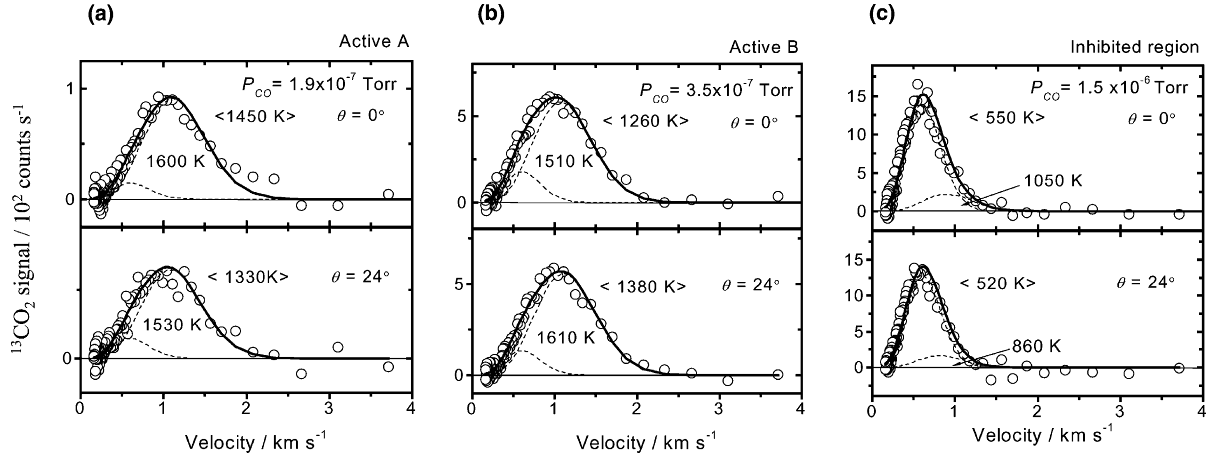

Fig. 3. Velocity distributions of desorbing CO_2 in three reaction zones: (a) active A, (b) active B, and (c) inhibited regions, at $T_S = 480$ K and $P_{O_2} = 1.0 \times 10^{-6}$ Torr. Typical deconvolutions are shown by broken curves. The temperature in $\langle\ \rangle$ was estimated from the mean translational energy.

of desorbing CO_2. The velocity distribution always showed a single peak although the sharpness changed significantly (Figs. 3a–c).

Above the KT, the velocity distribution was mostly described by a Maxwellian distribution at T_S regardless of the θ value. The distribution at $\theta = 0°$ involved a fast component of about 1050 ± 150 K. Its amount was about 15% or less. Here, the slow component described by a Maxwell distribution at T_S was fitted to the observed signal and the remaining signal after subtraction of the slow one was then fitted to a modified Maxwellian form. A typical deconvolution is shown by broken curves in the figure. The resultant energy of the fast component is indicated (in the temperature units) as $T_{\langle E\rangle} = \langle E\rangle/2k$, where $\langle E\rangle$ is the mean translational energy and k is the Boltzman constant. The thermalized component yields a cosine distribution and the angular distribution was then deconvoluted into a cosine form and a sharp component consisting of the remaining signal. Thus, the angular distribution in the inhibited region was approximated as $0.15\cos^4\theta + 0.85\cos\theta$. The fast component at 24° was reduced to about 70% and showed a temperature of 860 K.

In 'active A,' the velocity distribution involved a larger fast component. The average translational temperature reached 1450 K at $\theta = 0°$ and 1330 K at $\theta = 24°$, being consistent with the normally directed and sharp angular distribution. The temperature of the fast component was estimated to be 1600 ± 70 K at $\theta = 0°$. Thus, the angular distribution was deconvoluted into $0.05\cos^6\theta + 0.01\cos\theta$.

The velocity distribution in 'active B' is interesting because the average translational temperature reached 1380 K at $\theta = 24°$ and decreased to 1260 K at $\theta = 0°$. These velocity distributions indicate the presence of inclined desorption. In the same way as above, the fast component was estimated to have 1610 ± 50 K at $\theta = 24°$ and 1510 ± 40 K at $\theta = 0°$ (Fig. 3b). In this deconvolution, the thermalized component was maximized. However, as long as only these two components are considered, their fractions can be determined uniquely because of the significant difference in the peak position between them. Furthermore, the resultant fraction must fit the deconvolution of the angular distribution. Thus, the angular distribution in 'active B' was approximated as $0.42\cos^8(\theta + 24) + 0.42\cos^8(\theta - 24) + 0.12\cos\theta$.

In the other deconvolution, the fast component was divided into the normally directed and inclined components by assuming the same sharpness as the fast component in the active A for the normally directed one and the collimated angle of 24° for the inclined components consisting of the remaining signal. The distribution was approximated as $0.15\cos^6\theta + 0.26\cos^{11}(\theta + 24) + 0.26\cos^{11}(\theta - 24) + 0.2\cos\theta$. The slow component had to be included to fit with the velocity data below 0.7 km/s. The contribution from the fast and normally directed component could not be completely excluded because of the similar velocity distributions. However, the normally directed component was still minor.

On this surface, the observation of desorption from declining facets was obscured by the reactive CO_2 desorption from other places, the high contribution of the cosine component, and the relatively slow velocity of the fast component.

3.1.4. LEED study

Sharp changes in the LEED spot intensity were found in 'active B.' The well-known (2×2)p2mg-O structure [19] (Fig. 4c) appeared at low P_{CO}. With increasing the P_{CO}, the half-order spots due to the (1×2) structure (Fig. 4d) intensified at around the middle of the active region and disappeared above the KT (Fig. 4e). Their spot intensities were monitored by a CCD-video at the acceleration voltage of 70 eV. The intensity of the half-order spot at $(-1/2, 1)$ was maximized in 'active B.' Concomitantly, the integral order spots at $(0, 1)$ and $(-1, 1)$ decreased at the SS and increased steeply just below the KT. On the other hand, the intensity of the (2×2)p2mg at $(-1, -1/2)$ was fairly constant below the SS and was suppressed above it. Above the KT, a clear (1×1) pattern (Fig. 4e) was observed. Such intensity changes were observed in the range of $T_S = 430$–500 K (Figs. 4a, b). The surface structure sharply changed as $(2 \times 2)\text{p2mg-O} \rightarrow (1 \times 2) \rightarrow (1 \times 1)$. Both transformations were accelerated at higher T_S because both the increase and decrease of the (1×2) spot systematically shifted to lower P_{CO} from the SS or KT points with increasing T_S, as typically shown at 480 K in Fig. 4. The decrease

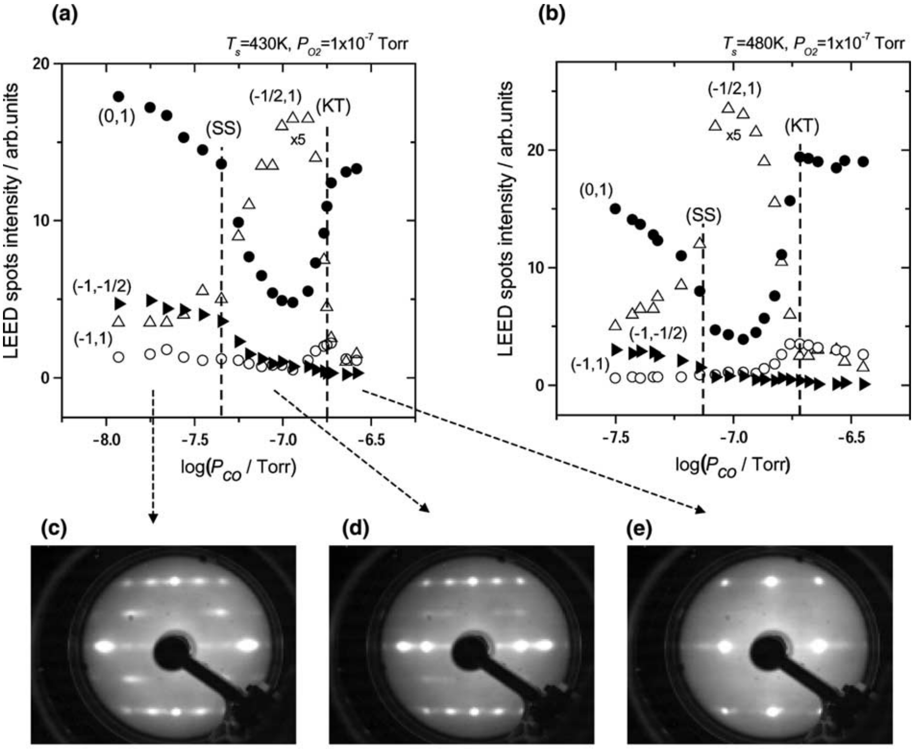

(2×2)p2mg (2×2)p2mg + (1×2) (1×1)

Fig. 4. Rh(1 1 0); spot intensities of (2×2)p2mg, (1×2), and (1×1) structures with CO pressures at fixed O_2 pressure of 1×10^{-7} Torr at (a) $T_S = 430$ K and (b) $T_S = 480$ K. The vertical lines indicate the site-switching and kinetic transition points. Typical LEED patterns at 430 K are shown for: (c) active A, (d) active B, and (e) inhibited regions. The accelerating voltage was 70 eV.

is controlled by the conversion of (1 × 2) after removal of oxygen and not by the accumulation of CO(a) [9]. The steady (0, 1) spot intensity above the KT increased with T_S, suggesting faster surface-atom orderings at higher T_S.

This (1 × 2) at the steady state did not return to the (1 × 1) by being heated to 600 K after removal of the reactant gasses. It yielded a (2 × 2)p2mg pattern, indicating the back diffusion of oxygen from the subsurface layer. On the other hand, the (1 × 2) structure, which was prepared by reduction with hydrogen after a short exposure to oxygen, was quickly converted into the (1 × 1) above 500 K. This indicates that the (1 × 2) at the steady state is not the same as the meta-stable missing-row form described previously [14]. The (1 × 2) at the steady state may be stabilized by oxygen in the subsurface layer. In fact, XPS measurements showed that the oxygen coverage in ‘active B’ was about half of the signal intensity in ‘active A,’ with (2 × 2)p2mg-O having a half monolayer of O(a) [14]. The intensity–voltage character of LEED showed remarkable differences in the accelerating voltage of 50–200 eV between both (1 × 2) structures.

3.2. Results on Pd(1 1 0)

On Pd(1 1 0), the rate increased linearly with increasing P_{CO} to the KT, where it dropped suddenly and showed negative orders in CO [9]. CO_2 desorption collimated along the surface normal below the KT, showing a $\cos^6\theta$ form along the [0 0 1] direction. Above the KT, it showed a cosine form. The velocity distribution curve involved two

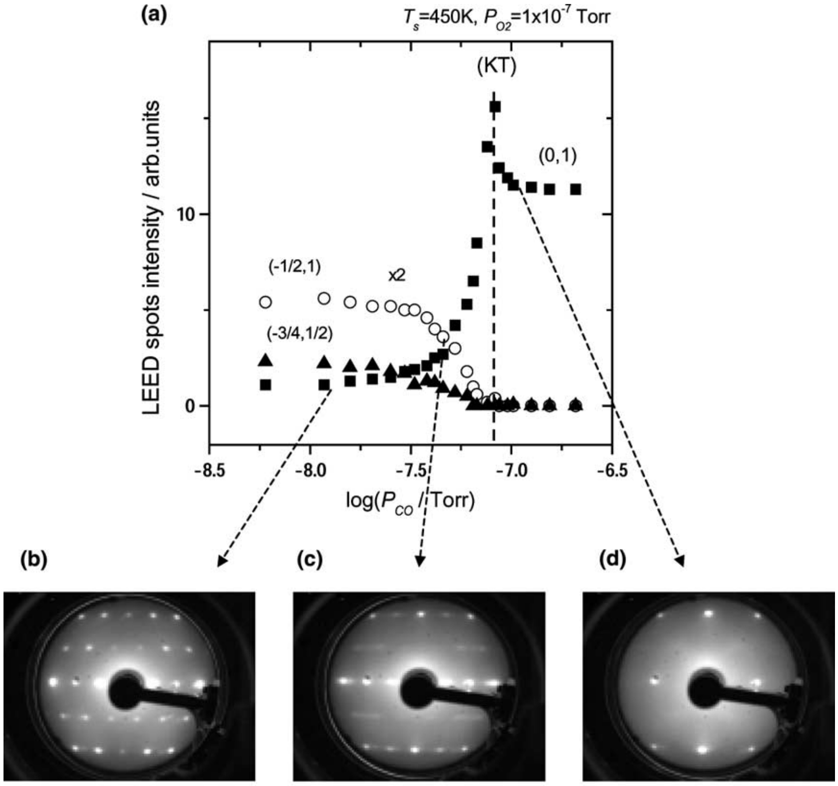

c(2 × 4) c(2 × 4) + (1 × 1) (1 × 1)

Fig. 5. Pd(1 1 0); (a) spot intensities of c(2 × 4)-O, (1 × 2)-CO, and (1 × 1) structures with CO pressures at fixed O_2 pressure of 1×10^{-7} Torr at $T_S = 450$ K and the accelerating voltage of 70 eV. The vertical lines indicate the kinetic transition point. Typical LEED patterns at 450 K are shown for (b) and (c) the active region and (d) the inhibited region.

desorption components, a fast one and a slow one. The former showed high translational energy and was suppressed above the KT. This component showed a $\cos^{10}\theta$ form. CO_2 desorption collimated sharply along the surface normal, similarly to that in 'active A' on Rh(1 1 0). No 'active B' was observed in the steady-state conditions on Pd(1 1 0).

LEED observations were consistent with the absence of bi-directional desorption. We monitored the LEED intensity on Pd(1 1 0) around the KT, as shown in Fig. 5. The LEED pattern changed from c(2 × 4)-O [12] into the (1 × 1) without passing the meta-stable (1 × 2) below the KT and showed the (1 × 1) or (1 × 2)-CO above the transition. No enhancement of the meta-stable (1 × 2) was found below the KT. Similar changes were observed in the temperature range of 360–460 K. This is consistent with the meta-stable (1 × 2), which can be prepared by oxygen removal with hydrogen and is converted into the (1 × 1) above 355 K [13].

4. Summary

On Rh(1 1 0), declining facets with a (1 1 1) structure on reconstructed (1 × 2) were confirmed to be active for a CO_2 formation process by means of LEED and product desorption dynamics. This active phase appears in the limited CO pressure range just below the kinetic transition in the steady-state CO oxidation. CO_2 desorption is split into bi-directional lobes collimated at ±24° off normal and the meta-stable (1 × 2) structure stabilized by oxygen provides declining CO_2 formation sites. On the other hand, on Pd(1 1 0), no meta-stable (1 × 2) structure is observed below the kinetic transition and the reconstructed (1 × 2) stabilized by oxygen is converted directly into the (1 × 1) form.

Acknowledgements

Rzeźnicka Izabela is indebted to the Ministry of Education, Science, Sports and Culture of Japan for her 2000–2004 scholarship. This work was supported in part by Grant-in-Aid No. 13640493 for General Scientific Research from the Japan Society for the Promotion of Science.

References

[1] F. Besenbacher, I. Stensgaard, in: D.A. King, D.P. Woodruff (Eds.), Chem. Phys. Solid Surf., Phase Transitions and Adsorbate Restructuring at Metal Surfaces, vol. 7, Elsevier, Amsterdam, 1994, p. 573.
[2] E.C. Sowa, M.A. van Hove, D.L. Adams, Surf. Sci. 199 (1988) 174.
[3] T. Matsushima, Heterogen. Chem. Rev. 2 (1995) 51.
[4] T. Matsushima, J. Chem. Phys. 93 (1990) 1464.
[5] T. Matsushima, Y. Ohno, K. Nagai, J. Chem. Phys. 94 (1991) 704.
[6] T. Matsushima, J. Chem. Phys. 91 (1989) 5722.
[7] T. Matsushima, Y. Ohno, Catal. Lett. 23 (1994) 313.
[8] I. Rzeznicka, L. Morales de la Garza, T. Matsushima, J. Vac. Sci. Technol. A 20 (2002) 1475.
[9] M.G. Moula, A.B.P. Mishra, I. Rzeznicka, M.U. Kislyuk, S. Liu, Y. Ohno, T. Matsushima, Chem. Phys. Lett. 341 (2001) 225.
[10] Md.G. Moula, S. Wako, G. Cao, K. Kimura, Y. Ohno, I. Kobal, T. Matsushima, Phys. Chem. Chem. Phys. 1 (1999) 3677.
[11] T. Engel, G. Ertl, Adv. Catal. 28 (1979) 1.
[12] H. Tanaka, J. Yoshinobu, M. Kawai, Surf. Sci. 327 (1995) L505.
[13] V.R. Dhank, G. Comelli, G. Paolucci, K.C. Prince, R. Rosei, Surf. Sci. 260 (1992) L24.
[14] V.R. Dhanak, G. Comelli, G. Cautero, G. Paolucci, K.C. Prince, M. Kiskinova, R. Rosei, Chem. Phys. Lett. 188 (1992) 237.
[15] C. Arich, F. Esch, G. Comelli, R. Rosei, J. Chem. Phys. 115 (2001) 477.
[16] T. Matsushima, D.B. Almy, J.M. White, Surf. Sci. 67 (1977) 89.
[17] G. Cao, Y. Seimiya, T. Matsushima, J. Mol. Catal. 141 (1999) 63.
[18] I. Kobal, I. Rzeźnicka, T. Matsushima, in: Recent Research Developments in Physical Chemistry, vol. 6, Transworld Research Network, 2002, p. 391.
[19] C. Comicioli, V.R. Dhank, G. Comelli, C. Astaldi, K.C. Prince, R. Rosei, A. Atrei, E. Zanazzi, Chem. Phys. Lett. 214 (1993) 438.